LETTERS

Unidirectional molecular motor on a gold surface

Richard A. van Delden[1], Matthijs K. J. ter Wiel[1], Michael M. Pollard[1], Javier Vicario[1], Nagatoshi Koumura[1] & Ben L. Feringa[1]

Molecules capable of mimicking the function of a wide range of mechanical devices have been fabricated, with motors that can induce mechanical movement attracting particular attention[1,2]. Such molecular motors convert light or chemical energy into directional rotary or linear motion[2–10], and are usually prepared and operated in solution. But if they are to be used as nanomachines that can do useful work, it seems essential to construct systems that can function on a surface, like a recently reported linear artificial muscle[11]. Surface-mounted rotors have been realized and limited directionality in their motion predicted[12,13]. Here we demonstrate that a light-driven molecular motor capable of repetitive unidirectional rotation[14] can be mounted on the surface of gold nanoparticles. The motor design[14] uses a chiral helical alkene with an upper half that serves as a propeller and is connected through a carbon–carbon double bond (the rotation axis) to a lower half that serves as a stator. The stator carries two thiol-functionalized 'legs', which then bind the entire motor molecule to a gold surface. NMR spectroscopy reveals that two photo-induced *cis–trans* isomerizations of the central double bond, each followed by a thermal helix inversion to prevent reverse rotation, induce a full and unidirectional 360° rotation of the propeller with respect to the surface-mounted lower half of the system.

Inspired by the ATP-ase system[15], we constructed an artificial surface-mounted motor schematically shown in Fig. 1a. The design of the motor molecule **1** is based on a second-generation[14] light-driven rotary motor **2** with a symmetric lower half bearing two methoxy substituents (Fig. 1b). Replacing these groups by two C_8-spacers terminated with thiols (as shown in structure **1**) allowed self-assembly onto a gold surface, providing **1-Au**. Gold nanoparticles are particularly appropriate for our purpose, as chromophore functionalized nanoparticles are well studied[16] and photochromism of azobenzenes[17] and electrochemical switching of rotaxanes[18] attached to such nanoparticles has been demonstrated. Two points of attachment are essential to prevent uncontrolled thermal rotation of the entire system with respect to the surface. The C_8-spacer should diminish direct (electronic) interaction between the chromophores and the Au surface (which might influence the excited state processes) and give the separate photoactive moieties sufficient free volume to perform the anticipated rotary motion. On the basis of the dynamic processes in structurally related molecular motors[14], **1-Au** was expected to exhibit photochemical and thermal isomerization processes, as shown in Fig. 1c.

Two energetically uphill photochemical isomerization steps (steps 1 and 3 in Fig. 1) each followed by an energetically downhill irreversible thermal helix inversion step (steps 2 and 4 in Fig. 1) result in a full 360° rotation of one half of the molecule with respect to the other. The direction of rotation is controlled by the configuration at the stereogenic centre. Crucial is a strong energetic preference for the methyl substituent to adopt a pseudo-axial orientation. Irradiation

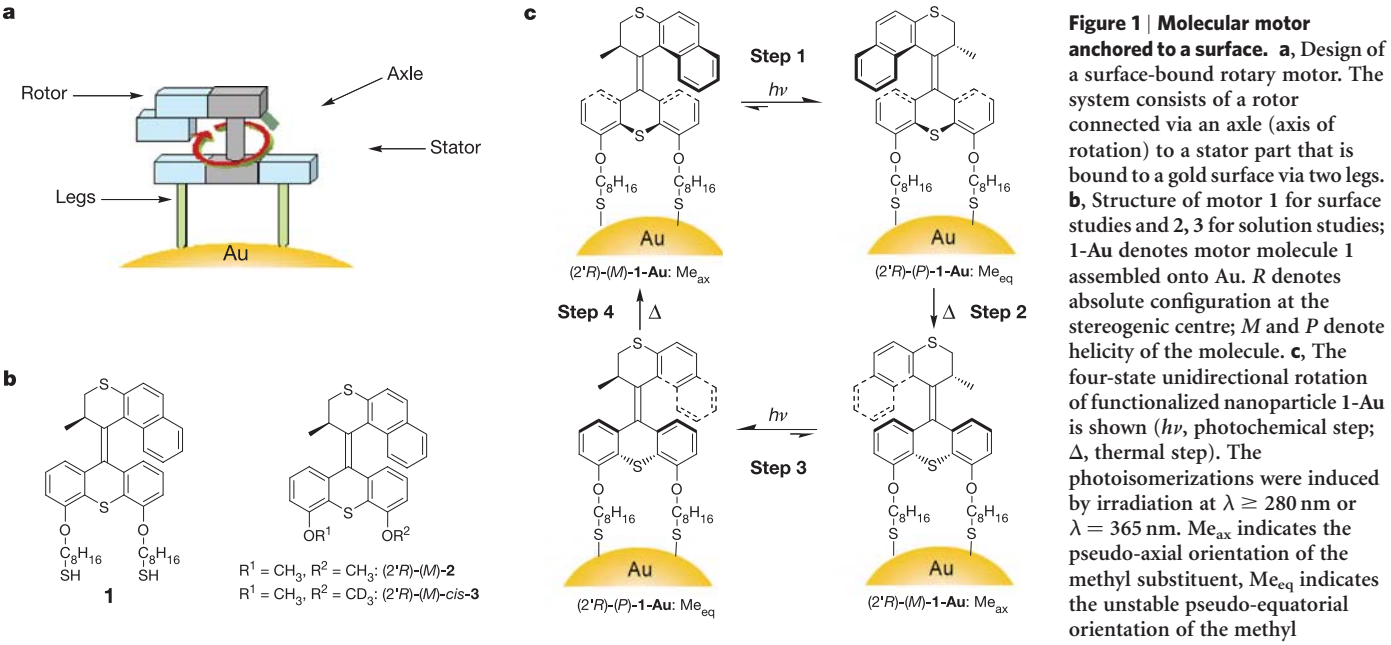

Figure 1 | Molecular motor anchored to a surface. **a**, Design of a surface-bound rotary motor. The system consists of a rotor connected via an axle (axis of rotation) to a stator part that is bound to a gold surface via two legs. **b**, Structure of motor 1 for surface studies and 2, 3 for solution studies; 1-Au denotes motor molecule 1 assembled onto Au. *R* denotes absolute configuration at the stereogenic centre; *M* and *P* denote helicity of the molecule. **c**, The four-state unidirectional rotation of functionalized nanoparticle 1-Au is shown (*hν*, photochemical step; Δ, thermal step). The photoisomerizations were induced by irradiation at $\lambda \geq 280$ nm or $\lambda = 365$ nm. Me_{ax} indicates the pseudo-axial orientation of the methyl substituent, Me_{eq} indicates the unstable pseudo-equatorial orientation of the methyl substituent.

[1]Department of Organic Chemistry, Stratingh Institute, University of Groningen, Nijenborgh 4, 9747 AG Groningen, The Netherlands.

of the stable (2′*R*)-(*M*)-isomer of **1-Au** with a pseudo-axial methyl substituent effects a *cis* → *trans* isomerization, which inverts the helicity of the system to form the (2′*R*)-(*P*)-isomer. Consequently, the methyl substituent is forced to adopt an energetically disfavoured pseudo-equatorial orientation. Upon heating, this unstable isomer undergoes a helix inversion resulting in the formation of the initial (2′*R*)-(*M*)-isomer, after a net 180° rotation of the upper half of the molecule in an anticlockwise fashion with respect to the lower half. This sequence is repeated in steps 3 and 4 to complete a full rotary cycle. The unidirectionality of the rotary process is ensured by the irreversibility of the thermal helix inversion steps.

Target compound **2** (4,5-dimethoxy-9-(2′,3′-dihydro-2′-methyl-1′*H*-naphtha[2,1-*b*]thiopyran-1′-ylidene)-9*H*-thioxanthene; Fig. 1b), which serves as a precursor and a solution phase model for **1-Au**, was synthesized by adapted methods used for second-generation motors[10]. The (2′*R*)-(*M*)-**2** stereoisomer was resolved by chiral high-performance liquid chromatography (HPLC) and the absolute stereochemistry unequivocally assigned based on circular dichroism (CD) spectroscopy and X-ray analysis (see Supplementary Table 1). Starting from (2′*R*)-(*M*)-**2**, deprotection of the methoxy-substituents and introduction of two octylthiol moieties was achieved by standard synthetic techniques. Nanoparticles (2′*R*)-(*M*)-**1-Au** were prepared by the Brust-Schiffrin method[19] and characterized by dynamic light scattering (DLS), transmission electron microscopy (TEM) (Supplementary Fig. 11), and spectroscopic methods (for ultraviolet/visible (UV/Vis) and CD spectroscopy see Fig. 2, and for additional CD, UV, NMR, Fourier transform infrared (FT-IR) and surface enhanced Raman spectroscopy, see Supplementary Figs 2, 3, 4, 7–9 and 10, respectively).

The UV/Vis and CD spectra of (2′*R*)-(*M*)-**1-Au** and (2′*R*)-(*M*)-**2** are characteristic of helical overcrowded alkenes (Fig. 2). The CD spectra of **1-Au** and **2** (Fig. 2a) are nearly identical because they solely reflect the helical chirality of the diaryl alkene moieties and confirm the (*M*)-helicity of **1-Au** and **2**. The UV/Vis spectrum of **1-Au** (Fig. 2b) is a superposition of the spectral bands of the motor moieties and a broad absorption of the nanoparticle, reaching far into the visible region (see Supplementary Fig. 2).

TEM data, together with the molar quantity of olefin moieties per gram of nanoparticles (as determined by CD spectroscopy) and the known density of gold ($19.3\,g\,cm^{-3}$)[20], gives the average overall formula of one nanoparticle of **1-Au**: $Au_{251}((S(CH_2)_8O)_2C_{27}H_{18}S_2)_{26}$. It can be calculated that for **1** there is only ~0.23 nm^2 surface area per linked sulphur atom; this can be compared with the surface area of alkanethiols on a flat Au surface as determined by electron diffraction studies ($0.214\,nm^2$)[21].

The combined photochemical and thermal processes were investigated spectroscopically in toluene solution. The presented data for **1-Au** are in full agreement with those of the parent (model and control) compound **2**, unless indicated.

A 1.035×10^{-5} M solution (chromophore concentration) of (2′*R*)-(*M*)-**1-Au** in toluene at room temperature was irradiated (wavelength $\lambda \geq 280$ nm) until a photostationary state (PSS) was reached. The approximate inversion of the CD spectrum upon irradiation (Fig. 2a) indicates the change in helicity going from (2′*R*)-(*M*)-**1-Au** to (2′*R*)-(*P*)-**1-Au** (step 1 in Fig. 1c). In the UV/Vis spectrum a decrease in the intensity of the high wavelength band is indicative of the formation of (2′*R*)-(*P*)-**1-Au** (Fig. 2b). Clear isosbestic point(s) in both CD and UV/Vis spectra for the photochemical and thermal steps support clean isomerization processes (Fig. 2). From the UV/Vis spectra of (2′*R*)-(*M*)-**2** and (2′*R*)-(*P*)-**2**, the ideal wavelength for the formation of the unstable isomer was determined to be 365 nm. Subsequent irradiation of (2′*R*)-(*M*)-**1-Au** at this wavelength indeed resulted in a more selective isomerization with an associated increase in intensity of the CD bands (Fig. 2a) and an anticipated PSS of approximately 94:6. UV/Vis and CD data are consistent with this observation (Fig. 2).

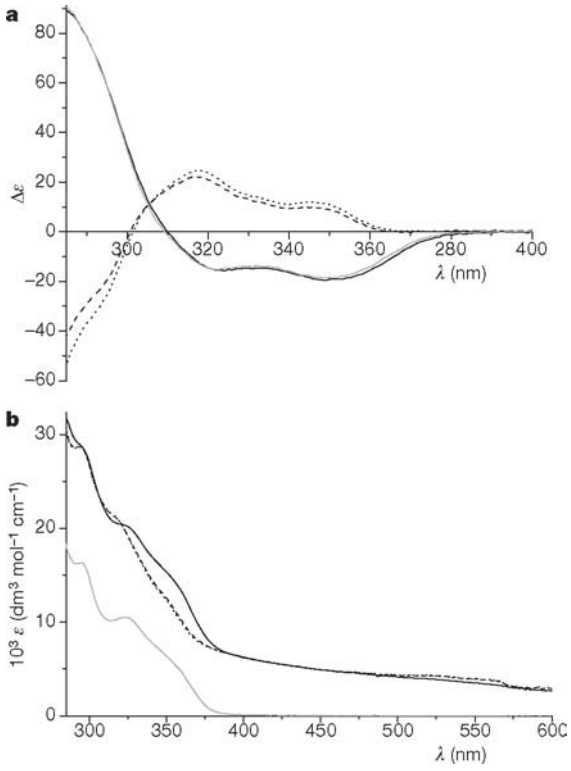

Figure 2 | CD and UV spectra of 1-Au and 2. CD (**a**) and UV/Vis (**b**) spectra of pure (2′*R*)-(*M*)-1-Au (solid black lines), $PSS_{\geq 280\,nm}$ (dashed black) and $PSS_{365\,nm}$ (dotted black) samples (all spectra are adjusted for molar concentration of chromophores), and CD (**a**) and UV/Vis (**b**) spectrum of (2′*R*)-(*M*)-2 (solid grey) in toluene. After heating of the PSS samples ($T > 50$ °C), the original spectra of (2′*R*)-(*M*)-1-Au and (2′*R*)-(*M*)-2 were obtained.

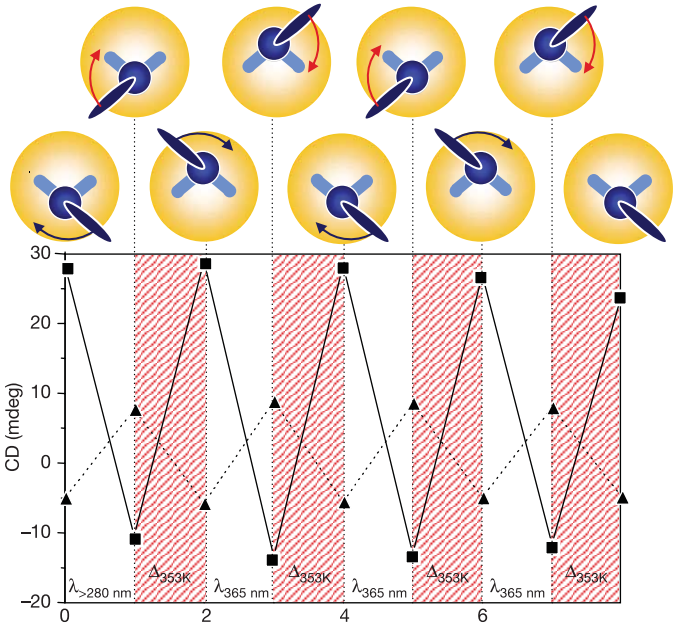

Figure 3 | Following two full turns by CD spectroscopy. Schematic representation of the unidirectional rotation of 1 (as viewed along the rotation axis) and two full four-stage 360° rotary cycles followed by CD spectroscopy. The change in CD intensity (mdeg) at 290 nm (solid line) and 320 nm (dashed) at each photochemical ($h\nu_{\lambda>280\,nm}$ and $h\nu_{\lambda=365\,nm}$) and thermal (Δ_{353K}) isomerization step is shown.

Subsequent heating of the PSS sample of (2′*R*)-(*P*)-**1-Au** ($T \geq 50\,^{\circ}C$) resulted in full conversion of unstable (2′*R*)-(*P*)-**1-Au** to stable (2′*R*)-(*M*)-**1-Au**, as a result of the thermal helix inversion (step 2 in Fig. 1c). It was verified that rotary motion occurs while motor **1-Au** remains bound to the surface; this was indicated by the presence of exclusively broad signals in the ^{1}H NMR spectrum (no trace of free motor in solution could be detected) after either heating the sample at 70 °C for 2 h or irradiation for 3 h at 365 nm. Subsequent KCN mediated etching of the gold core of this sample of **1-Au** after 3 h irradiation at 365 nm revealed unbound unstable and stable motor in a 2.5:1 ratio.

The kinetics of this helix inversion were determined by monitoring the change in CD intensity with time at various temperatures ($T = 323, 333, 343, 353$ K), providing the rate constant (k_t) which was used to calculate the Gibbs free energy of activation ($\Delta^{\ddagger}G^{\circ} = 96 \pm 2\,kJ\,mol^{-1}$) for the (2′*R*)-(*P*)-**1-Au** to (2′*R*)-(*M*)-**1-Au** interconversion using the Eyring equation. The slightly higher barrier than found for **2** in solution ($\Delta^{\ddagger}G^{\circ} = 94 \pm 2\,kJ\,mol^{-1}$) can be attributed to the reduction in the degrees of freedom of the molecule when grafted onto the Au surface. At room temperature (293 K), the half-life for thermal helix inversion has almost doubled going from **2** ($t_{\frac{1}{2}} = 56 \times 10^{2}$ s) to **1-Au** ($t_{\frac{1}{2}} = 12 \times 10^{3}$ s). After the light-induced energetically uphill process (2′*R*)-(*M*)-**1-Au** to (2′*R*)-(*P*)-**1-Au** (step 1 in Fig. 1c) followed by a thermal energetically

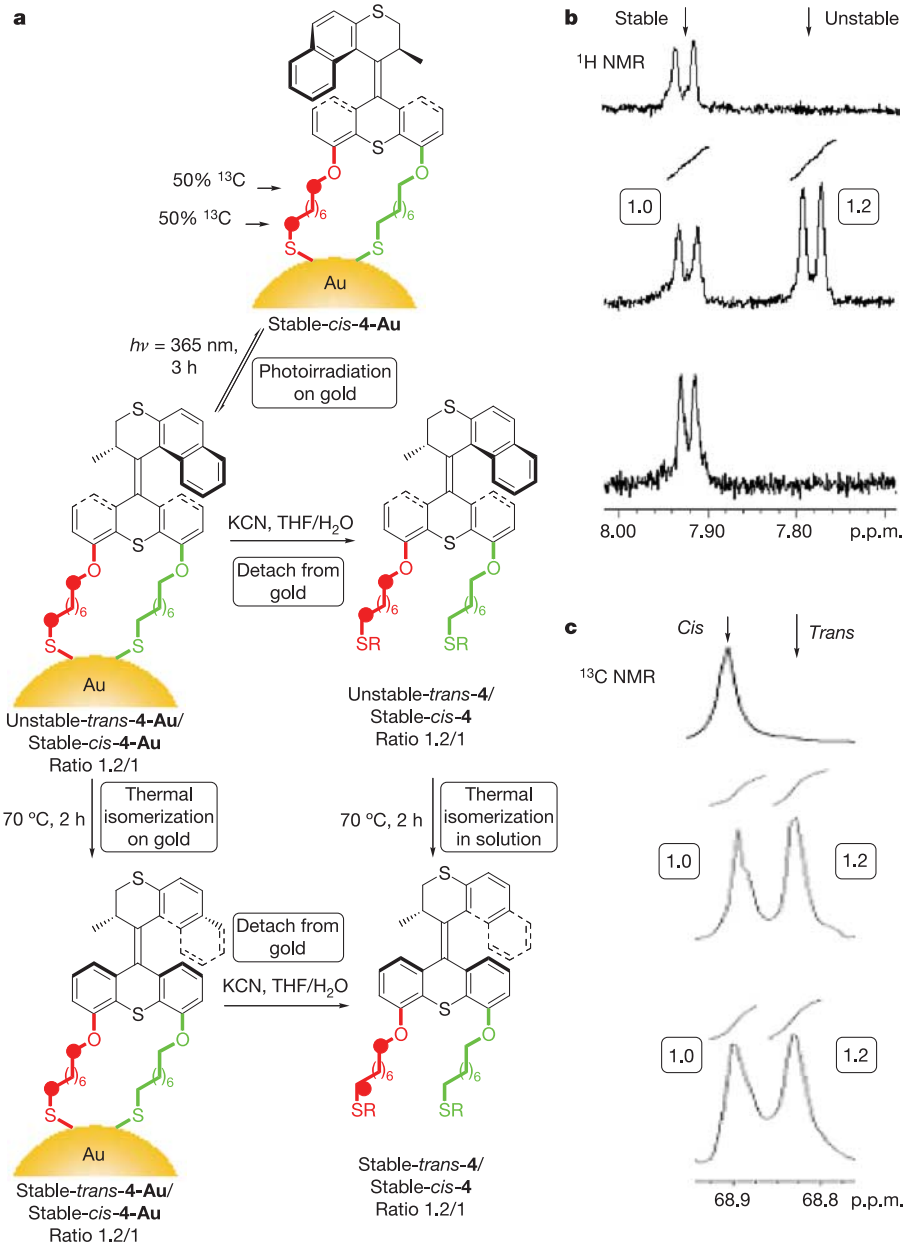

Figure 4 | Confirmation of unidirectional rotation on the nanoparticle using NMR spectroscopy. a, Photochemical and thermal isomerization of ^{13}C isotope labelled motor 4 on gold (4-Au) and structures of major isomers of 4-Au. Cleaved motor probably exists as a mixture of free thiol (R = H) and disulphide (R = S-Motor). **b**, Key signals (Ar*H*) in the ^{1}H NMR of stable-*cis*-4 in solution (top panel), after irradiation of stable-*cis*-4-Au and core etching (middle panel) and after irradiation of stable-*cis*-4-Au, heating, then etching (bottom panel). **c**, Key signals (-O^{13}*C*H$_2$[CH$_2$]$_7$) in the ^{13}C NMR of stable-*cis*-4 in solution (top panel), after irradiation of stable-*cis*-4-Au and core etching, and subsequent heating (middle panel), and after irradiation of stable-*cis*-4-Au, heating, then etching (bottom panel). The conversion of stable isomer 4-Au to unstable isomer 4-Au (evaluated by ^{1}H NMR) matched the final conversion of stable-*cis*-4-Au to stable-*trans*-4-Au evaluated by ^{13}C NMR. In both cases, NMR analysis was performed after detachment.

downhill helix inversion (2′*R*)-(*P*)-**1-Au** to (2′*R*)-(*M*)-**1-Au** (step 2 in Fig. 1c), the upper rotor half of the molecule has performed a half rotation in an anticlockwise direction with respect to the lower half. Performing the same two-step process repeatedly results in continual unidirectional rotary motion. The state of the motor can be followed by CD spectroscopy, as is shown (Fig. 3) for two consecutive 360° cycles.

To confirm that the introduction of the two legs in the lower part of the molecule does not affect the four-stage unidirectional rotary process, we studied (2′*R*)-(*M*)-**3**, which has a non-symmetrical lower part with one OCH_3 and one OCD_3 (see Fig. 1b). These groups have negligible influence on the photochemical and thermal behaviour, and allowed the detection by NMR of all four steps in the rotary cycle (see Supplementary Information, Section 3).

Unequivocal proof for the unidirectionality of the motor attached to gold nanoparticles was achieved with isotope labelled motor **4-Au** (Fig. 4). The only difference between **1-Au** and **4-Au** is that one leg in the latter compound contains a ^{13}C isotope at the two positions flanking the stator and the surface bound thiol. The two distinct legs created in this way allow accurate detection by ^{1}H and ^{13}C NMR of the isomers after photochemical and thermal steps on the surface, as illustrated in Fig. 4a.

The stable *cis*-isomer of **4** bound to the gold (*cis*-**4-Au**) was irradiated at 365 nm wavelength, and the sample split into two portions. The first portion was treated (KCN/THF/H_2O) so as to detach the motor from the surface to provide a mixture of the *trans*-unstable-**4** and *cis*-stable-**4** (ratio 1.2:1, ^{1}H NMR analysis, Fig. 4b). Subsequent thermal isomerization in toluene solution resulted in stable *trans*-**4** and stable-*cis*-**4** isomers (1.2:1 ratio, ^{13}C NMR analysis Fig. 4c).

The second portion was heated (70 °C, 2 h) to induce thermal isomerization of the motor while still on the gold surface (unstable-*trans*-**4-Au** to stable-*trans*-**4-Au**). Subsequent cleavage (KCN/THF/H_2O) of the motor from the gold provided an identical mixture of stable-*trans*-**4** and stable-*cis*-**4**. These data show that the photochemical conversion of the stable form of **4-Au** to the unstable form of **4-Au** (^{1}H NMR analysis) correlates perfectly with the formation of stable *trans*-**4-Au** from stable *cis*-**4-Au** (^{13}C NMR analysis).

The combined results (from CD studies of optically active (2′*R*)-(*M*)-**1-Au**, and NMR studies of ^{13}C isotopically labelled **4-Au**, with distinct legs) provide compelling evidence for the unidirectionality of the rotary process on the surface. We expect that the successful formation of fully functional surface-mounted rotors will enable investigation of the concerted action of a large ensemble of unidirectional molecular motors, and that this system might be a first step towards the construction of more elaborate and functional nanosized mechanical devices.

Received 12 July; accepted 2 August 2005.

1. Balzani, V., Venturi, M. & Credi, A. *Molecular Devices and Machines—A Journey into the Nanoworld* (Wiley-VCH, Weinheim, 2003).
2. van Delden, R. A., ter Wiel, M. K. J., Koumura, N. & Feringa, B. L. in *Molecular Motors* (ed. Schliwa, M.) Ch. 23, 559–577 (Wiley-VCH, Weinheim, 2003).
3. Koumura, N., Zijlstra, R. W. J., van Delden, R. A., Harada, N. & Feringa, B. L. Light-driven monodirectional molecular rotor. *Nature* **401,** 152–155 (1999).
4. Kelly, T. R., De Silva, H. & Silva, R. A. Unidirectional rotary motion in a molecular system. *Nature* **401,** 150–152 (1999).
5. Leigh, D. A., Wong, J. K. Y., Dehez, F. & Zerbetto, F. Unidirectional rotation in a mechanically interlocked molecular rotor. *Nature* **424,** 174–179 (2003).
6. Anelli, P. L., Spencer, N. & Stoddart, J. F. A molecular shuttle. *J. Am. Chem. Soc.* **113,** 5131–5133 (1991).
7. Sherman, W. B. & Seeman, N. C. A precisely controlled DNA biped walking device. *Nano Lett.* **4,** 1203–1207 (2004).
8. Sauvage, J.-P. (ed.) *Molecular Machines and Motors* (Structure and Bonding, Vol. 99, Springer, Berlin, 2001).
9. van Delden, R. A., Koumura, N., Harada, N. & Feringa, B. L. Unidirectional rotary motion in a liquid crystalline environment; colour tuning by a molecular motor. *Proc. Natl Acad. Sci. USA* **99,** 4945–4949 (2002).
10. Koumura, N., Geertsema, E. M., van Gelder, M. B., Meetsma, A. & Feringa, B. L. Second generation light-driven molecular motors. Unidirectional rotation controlled by a single stereogenic center with near-perfect photoequilibria and acceleration of the speed of rotation by structural modification. *J. Am. Chem. Soc.* **124,** 5037–5051 (2002).
11. Liu, Y. *et al.* Linear artificial muscles. *J. Am. Chem. Soc.* **127,** 9745–9759 (2005).
12. Zheng, X. *et al.* Dipolar and nonpolar altitudinal molecular rotors mounted on an Au(111) surface. *J. Am. Chem. Soc.* **126,** 4540–4542 (2004).
13. Kottas, G. S., Clarke, L. I. & Horinek, D. Michl, J. Artificial molecular rotors. *Chem. Rev.* **105,** 1281–1376 (2005).
14. Koumura, N., Geertsema, E. M., Meetsma, A. & Feringa, B. L. Light-driven molecular rotor: unidirectional rotation controlled by a single stereogenic center. *J. Am. Chem. Soc.* **122,** 12005–12006 (2000).
15. Noji, H., Yasuda, R., Yoshida, M. & Kinosita, K. Direct observation of the rotation of F_1-ATPase. *Nature* **386,** 299–302 (1997).
16. George Thomas, K. & Kamat, P. V. Chromophore-functionalised gold nanoparticles. *Acc. Chem. Res.* **36,** 888–898 (2003).
17. Manna, A. *et al.* Optimised photoisomerisation on gold nanoparticles capped by unsymmetrical azobenzene disulfides. *Chem. Mater.* **15,** 20–28 (2003).
18. Long, B., Nikitin, K. & Fitzmaurice, D. Assembly of an electronically switchable rotaxane on the surface of a titanium dioxide nanoparticle. *J. Am. Chem. Soc.* **125,** 15490–15498 (2003).
19. Brust, M., Walker, M., Behell, D., Schiffrin, D. J. & Whyman, R. J. Synthesis of thiol-derivatised gold nanoparticles in a 2-phase liquid-liquid system. *Chem. Soc. Chem. Comm.*, 801–802 (1994).
20. Lide, D. R. (ed.) *CRC Handbook of Chemistry and Physics 2003–2004* 84th edn 4–59 (CRC Press, Boca Raton, 2003).
21. Ullman, A. Formation and structure of self-assembled monolayers. *Chem. Rev.* **96,** 1533–1554 (1996).

Supplementary Information is linked to the online version of the paper at www.nature.com/nature.

Acknowledgements We thank C. R. van den Brom for performing the TEM measurements described, A. Meetsma for X-ray analysis and J. G. McGarvey for access to Raman facilities. Financial support from the Netherlands Organisation for Scientific Research (NWO-CW), the Materials Science Centre, and the University of Groningen is acknowledged. J.V. thanks the Departamento de Educación, Universidades e Investigación del Gobierno Vasco, for a postdoctoral fellowship.

Author Information Reprints and permissions information is available at npg.nature.com/reprintsandpermissions. The authors declare no competing financial interests. Correspondence and requests for materials should be addressed to B.L.F. (B.L.Feringa@rug.nl).